The dark matter halo shape of edge-on disk galaxies

IV. UGC 7321

J.C. O'Brien[1], K.C. Freeman[1] and P.C. van der Kruit[2]

[1] Research School of Astronomy and Astrophysics, Australian National University, Mount Stromlo Observatory, Cotter Road, ACT 2611, Australia
e-mail: jesscobrien@gmail.com; kcf@mso.anu.edu.au*
[2] Kapteyn Astronomical Inst[Bitute, University of Groningen, P.O. Box 800, 9700 AV Groningen, the Netherlands
e-mail: vdkruit@astro.rug.nl*

Received Xxxxxxx 00, 2010; accepted Xxxxxxx 00, 2010

ABSTRACT

This is the fourth paper in a series in which we attempt to put constraints on the flattening of dark halos in disk galaxies. We observed for this purpose the HI in edge-on galaxies, where it is in principle possible to measure the force field in the halo vertically and radially from gas layer flaring and rotation curve decomposition respectively. As reported in earlier papers in this series we have for this purpose analysed the HI channel maps to accurately measure all four functions that describe as a function of galactocentric radius the planar HI kinematics and 3D HI distribution of a galaxy: the radial HI surface density, the HI vertical thickness, the rotation curve and the HI velocity dispersion. In this paper we analyse these data for the edge-on galaxy UGC7321.
We measured the stellar mass distribution ($M = 3\times10^8$ M$_\odot$with $M/L_R \lesssim 0.2$), finding that the vertical force of the gas disk dominates the stellar disk at all radii. Measurements of both the rotation curve and the vertical force field showed that the vertical force puts a much stronger constraint on the stellar mass-to-light ratio than rotation curve decomposition. Fitting of the vertical force field derived from the flaring of the HI layer and HI velocity dispersion revealed that UGC7321 has a spherical halo density distribution with a flattening of $q = c/a = 1.0 \pm 0.1$. However, the shape of the vertical force field showed that a non-singular isothermal halo was required, assuming a vertically isothermal HI velocity dispersion. A pseudo-isothermal halo and a gaseous disk with a declining HI velocity dispersion at high latitudes may also fit the vertical force field of UGC7321, but to date there is no observational evidence that the HI velocity dispersion declines away from the galactic plane. We compare the halo flattening of UGC7321 with other studies in the literature and discuss its implications. Our result is consistent with new n-body simulations which show that inclusion of hydrodynamical modelling produces more spherical halos.

Key words. galaxies: structure; galaxies: kinematics and dynamics; galaxies: halos; galaxies: ISM

1. Introduction

In paper I in this series (O'Brien et al., 2010a) we presented HI observations of a sample of 8 edge-on, HI rich, late-type galaxies. The aim of the project has been described there in detail. Briefly, we attempt to put constraints on the flattening of dark halos around disk galaxies by measuring the force field of the halo vertically from the flaring of the HI layer and radially from rotation curve decomposition. For the vertical force field we need to determine in these galaxies both the velocity dispersion of the HI gas (preferably as a function of height from the central plane of the disk) and the thickness of the HI layer, all of this as a function of galactocentric radius. In addition we also need to extract information on the rotation of the galaxy and the deprojected HI surface density, also as a function of galactocentric radius.

In paper II (O'Brien et al., 2010b) we discussed methods to analyse the HI observations in edge-on galaxies and presented a new method to measure the radial distributions, rotation curves and velocity dispersions. We applied this method to our sample of galaxies in the third paper in this series: O'Brien et al. (2010c). In that paper we also developed a new method to derive the thickness of the HI layer, or 'flaring profile', as a function of galactocentric radius, which we used to measure the HI flaring of each galaxy in our sample.

In the present paper we have fitted the vertical shape $q = c/a$ of the halo density distribution for the northern galaxy UGC7321. This particular system was chosen as a first application since the sensitivity of the HI imaging obtained for UGC7321 at the VLA was 5 times greater than that for the southern galaxies that we observed with the ATCA, allowing more accurate measurement of the gas layer flaring to high latitudes, and better measurement of the HI velocity dispersion. Due to its northern location, UGC7321 was not in our initial southern galaxy sample for which we measured near-IR and optical stellar photometry at Siding Spring Observatory. However, VLA HI data observed by Lyn Matthews (Matthews et al., 1999) was available for this galaxy and Michael Pohlen (Pohlen et al., 2002) kindly supplied *R*-band photometry which allowed us to derive the stellar luminosity density necessary to analyse the halo density distribution.

In Sect. 2 we present the surface brightness and deprojected luminosity volume density, and our derivation of the halo core radius, halo asymptotic velocity, and stellar mass-to-light ratio by rotation curve decomposition. In Sect. 3, we present a new simple method used to measure the halo shape using the vertical gradient of the vertical force, dK_z/dz, with the usual assumption of gas in hydrostatic equilibrium to determine the total

* For correspondence contact Ken Freeman or Piet van der Kruit

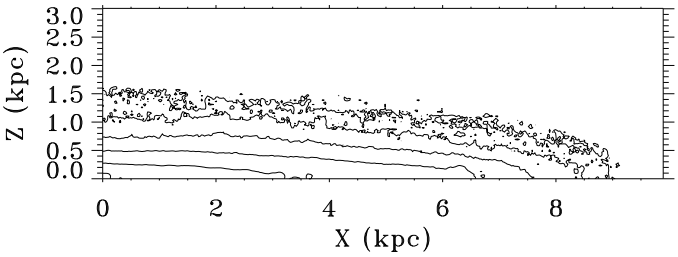

Fig. 1. Projected stellar surface density of UGC7321 averaged over all quadrants. Contours are separated on a log scale at 0.1, 0.3, 1, 3, 10, 30 $L_{\odot}pc^{-2}$.

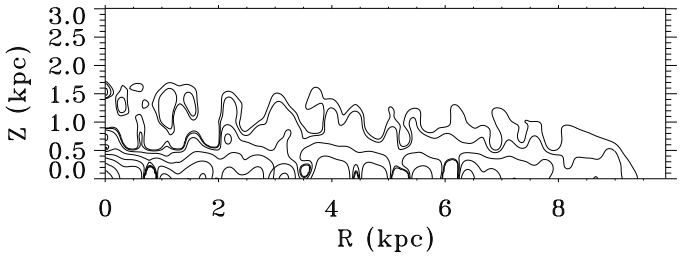

Fig. 2. Stellar luminosity volume density in R and z after deprojecting the observed surface density using the Inverse Abel Integral. Contours are separated on a log scale at 0.0001, 0.003, 0.001, 0.003, 0.01, 0.03, 0.1, 0.3 $L_{\odot}pc^{-3}$. The radial and vertical scalelengths, as shown in Fig. 3, are h_R = 2.65 kpc and h_z = 245 pc.

dK_z/dz of the galaxy. The resulting halo shape measurement for UGC7321 is presented and discussed in Sect. 4, and compared to other measurements of dark halo flattening in Sect. 5. Sect. 6 summarizes our conclusions.

2. Stellar surface brightness and deprojected luminosity density of UGC7321

Fig. 1 shows the R-band surface brightness – averaged over four quadrants – of UGC7321 with contours ranging from 0.1 to 30 $L_{\odot}pc^{-2}$ in steps of 0.5 dex. The observations and photometric calibration of UGC7321 are discussed in Pohlen et al. (2002). Pohlen et al. (2003) analysed the projected surface brightness showing peanut-shaped deviations from elliptical fits to the isophotes at z heights greater than 0.5 kpc above the plane. These deviations provide strong evidence of a stellar bar, although it is difficult to measure the scale of the bar from the scale of the boxy-peanut shaped bulge (Athanassoula, private communication).

Using an exponential radial surface profile we fit the central surface brightness and apparent radial scale length of the projected surface density. In logarithmic units

$$\mu(X) = \mu_0 + 1.086(X/h_X) \ \text{mag arcsec}^{-2}, \quad (1)$$

where X denotes the major axis distance. We found the projected central R-band surface brightness to be 22.0 mag arcsec^{-2}, with a scalelength of 4.0 ± 0.3 kpc, in agreement with that measured by Pohlen et al. (2003). The projected central surface brightness is consistent with the B and R-band measurement by Matthews et al. (1999) when the internal extinction model that Matthews et al. used is factored in. The projected surface brightness shows a small nuclear feature smaller than 1 kpc, and an exponential profile from 0.5 to 6.5 kpc, declining steeply after 7 kpc.

2.1. Deprojection

To deproject the luminosity distribution from the edge-on projection, we assume azimuthal symmetry and perform a direct deprojection of the projected surface density on the sky using the inverse Abel transform

$$I(R,z) = \frac{-1}{\pi} \int_R^{\infty} \frac{1}{\sqrt{X^2 - R^2}} \frac{dI(X,z)}{dX} dX, \quad (2)$$

where X is the position along the major axis and R is the galactocentric radius in the cylindrical coordinate system. Applying the inverse Abel tranform to each z-plane yields the luminous volume density $I(R,z)$ of the galaxy in $L_{\odot}pc^{-3}$ as a function of cylindrical radius R and height z. To minimise the incidence of local regions with a negative derivative $dI(X,z)/dX$, we performed the deprojection after smoothing the projected surface density by several different 2D Gaussians with FWHM ranging from 256 pc to 1027 pc (or 10 and 40 pixels, respectively).

Fig. 2 shows the derived volume density $I(R,z)$ of UGC7321, while Fig. 3 shows the radial and vertical surface brightness obtained by integrating over the volume density. UGC7321 is indeed a very low surface brightness galaxy. The face-on radial scalelength is h_R = 2.65 ± 0.17 kpc. Both the volume density and the radial profile, show that UGC7321 clearly has a small central nuclear region that is approximately 8 times brighter in surface brightness than the fitted central surface brightness of μ_R = 23.4 ± 0.14 mag arcsec^{-2} derived assuming an exponential disk only. The peak face-on central surface brightness of the nuclear region is μ_R = 21.1 mag arcsec^{-2}.

The central luminosity volume density of UGC7321 is 0.3 $L_{\odot}pc^{-3}$ in the central nucleus averaged over 250 pc. At 2.2 scalelengths the midplane volume density is 0.002 $L_{\odot}pc^{-3}$, much less than the luminosity density near the Sun (≈ 0.1 $L_{\odot}pc^{-2}$) as would be expected for such a low surface brightness galaxy.

2.2. Rotation curve decomposition

In the standard manner we decomposed the rotation curve to obtain the parameters of a spherical pseudo-isothermal halo, and constrain the stellar mass-to-light ratio. The radial surface density of the stars and gas was used directly to derive the rotation curve contribution due to each luminous mass component, and the observed rotation curve fitted such that

$$v_h^2 = v_{obs}^2 - \left(v_s^2 + v_g^2\right), \quad (3)$$

where $v_{obs}(R)$ is the observed rotation curve, and $v_h(R)$, $v_s(R)$ and $v_g(R)$ are the rotation due to the halo, stellar and gas mass components, respectively. The radial surface density of each luminous component was obtained by integrating over z, and a constant R-band stellar M/L_R was adopted. The HI surface density was scaled by a factor of 1.4 to include He and (a minimal amount of) molecular gas.

The observed rotation curve was fitted using a spherical pseudo-isothermal halo density distribution

$$\rho_h(R) = \rho_{h,0} \frac{R_c^2}{R^2 + R_c^2} \quad (4)$$

with corresponding rotation curve

$$v_h^2(R) = 4\pi G \rho_{h,0} R_c^2 \left[1 - \frac{R_c}{R} \arctan\left(\frac{R}{R_c}\right)\right]. \quad (5)$$

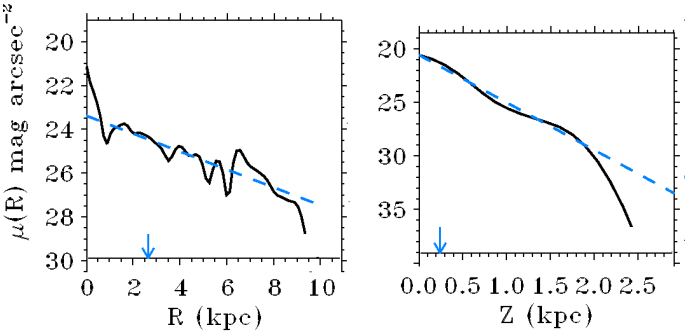

Fig. 3. Exponential fits to the radial and vertical surface brightness profiles formed by integrating over the deprojected volume density. The arrows mark the radial scalelength (left) and vertical scaleheight (right).

The pseudo-isothermal halo shown above is defined by the core radius R_c and central density $\rho_{h,0}$, and asymptotes at $R \to \infty$ to

$$v_{h,\infty}^2 = 4\pi G \rho_{h,0} R_c^2, \tag{6}$$

such that the rotation can also be written

$$v_h^2(R) = v_{h,\infty}^2 \left[1 - \frac{R_c}{R} \arctan\left(\frac{R}{R_c}\right)\right]. \tag{7}$$

By definition the rotation curve measures the total force in the radial direction $K_R = v^2(R)/R$; however it is unable to constrain the halo flattening q.

By evaluating the radial force $K_R(R,z)$ of a flattened pseudo-isothermal halo with density distribution

$$\rho(R,z) = \frac{\rho_{h,0} R_c^2}{R_c^2 + R^2 + z^2/q^2}, \tag{8}$$

Sackett et al. (1994) show that the corresponding rotation curve in the midplane is

$$v_h^2(R,q) = v_{h,\infty}^2(q) \left[1 - \frac{\gamma}{\arctan\gamma} \left(\frac{q^2 R_c^2}{R^2 + a}\right)^{1/2} \arctan\left(\frac{R^2 + a}{q^2 R_c^2}\right)^{1/2}\right], \tag{9}$$

where

$$\gamma = \frac{\sqrt{1-q^2}}{q} \quad ; \quad a = (1-q^2) R_c^2 \tag{10}$$

and the asymptotic rotation $v_{h,\infty}^2(q)$ is very similar to the asymptotic rotation of a spherical isothermal halo with

$$v_{h,\infty}^2(q) = 4\pi G \rho_{h,0} R_c^2 f(q), \tag{11}$$

where

$$f(q) = \frac{q}{\sqrt{1-q^2}} \arccos(q). \tag{12}$$

We use the rotation curve of a spherical pseudo-isothermal halo, as the shape of the rotation of a similar, but flattened halo is almost the same. This similarity implies that the measured asymptotic rotation derived from a spherical pseudo-isothermal fit to the rotation curve also defines the asymptotic rotation of a flattened pseudo-isothermal halo via Eqn. (11).

In Fig. 4 we show how the rotation curve of a flattened pseudo-isothermal halo varies with q (for $q \leq 1$) at z=0. The

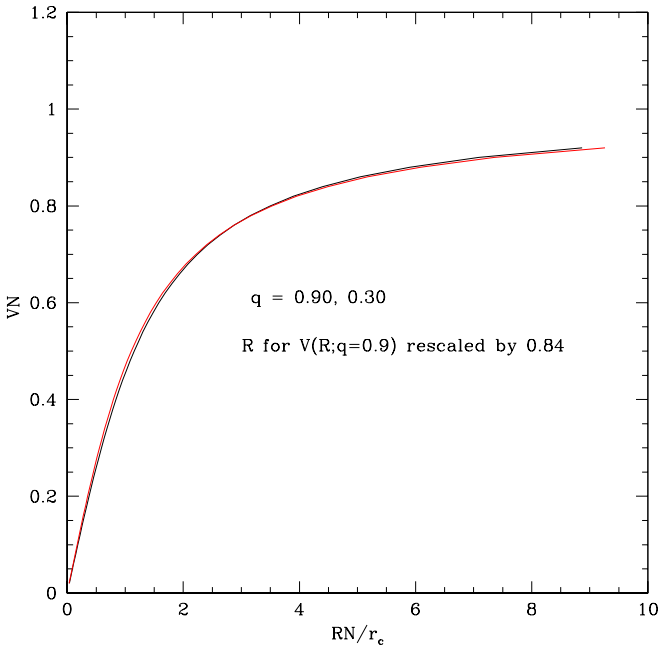

Fig. 4. Scaled rotation curves of a flattening pseudo-isothermal halo for two different values of the halo flattening q. The thick, black curve shows the rotation curve of $q = 0.3$ and the thin, red curve shows the rotation for $q = 0.9$ with the radius scaled by 0.84. The vertical axis shows the rotation normalised by the asymptotic rotation $v_{h,\infty}(q)$, while the abscissa shows the radius normalised by the core radius R_c. The nearly identical shape of the two curves shows that shape of the rotation curve of the halo is almost independent of q, with the radial scaling varying by a constant factor (of only $\approx$ 15% in this case) over a large range of q.

vertical axis shows the rotation normalised by the asymptotic rotation $v_{h,\infty}(q)$, while the abscissa shows the radius normalised by the core radius R_c. The thick, black curve shows the rotation for $q = 0.3$, while the thin, red curve shows the rotation for $q = 0.9$ with the radius scaled by 0.84. The nearly identical shape of the two curves shows that shape of the rotation curve of the halo is almost independent of q, with the radial scaling varying by only $\approx$ 15% over a large range of q. The derived halo central density does vary significantly with q, becoming denser for more flattened halos:

$$\rho_{h,0}(q) = \frac{v_{h,\infty}^2(q=1)}{4\pi G} \frac{1}{R_c^2 f(q)}, \tag{13}$$

In Sect. 4 we measure q by fitting the gradient of the vertical force dK_z/dz, where the gradient of the flattened pseudo-isothermal halo is also given by Sackett et al. (1994). As $K_z(R,z)$ also depends on the same parameters q, halo core radius R_c and halo central density $\rho_{h,0}$, we can use the asymptotic halo rotation $v_{h,\infty}$ and the core radius R_c which are well measured from rotation curve decomposition, and just perform a single parameter fit to the flattening q, as the central density $\rho_{h,0}$ is tied to $v_{h,\infty}$, R_c and q.

In Fig. 5 we show the best fitting stellar and halo rotation curves derived from rotation curve decomposition of UGC7321. The observed rotation curve is shown by the thick black line, while the rotation due to gas, stars and the halo are shown by dashed lines (from the bottom up stars (red), gas (green) and halo (blue). The resulting fit is shown by the grey full-drawn line (yellow). The best fit was achieved with a sub-maximal (see

below) stellar M/L_R of 1.05, which scaled the stellar component from a luminosity of $L = 4.0 \times 10^8$ $L_\odot$ to a mass of 4.2×10^8 $M_\odot$. UGC7321 is a gas-rich low surface brightness galaxy with a $M_{HI}/L_R = 2.2$; thus even with an M/L_R near unity, the stellar mass is roughly a third of the gas mass ($M_g = 1.4 M_{HI}$).

The plot shows that the rotation curve is well fit by a pseudo-isothermal halo with core radius $R_c = 0.52 \pm 0.02$ kpc, and central density $\rho_{h,0} = 0.73 \pm 0.05$ $M_\odot pc^{-3}$. As the halo core radius and halo asymptotic rotation are nearly independent of the halo shape in flattened pseudo-isothermal halos, we adopt those measurements from rotation curve decomposition for our halo shape modelling in Sect. 3. The halo is clearly the dominant component at all radii, comprising over 90% of the total galaxy mass of 3.2×10^{10} $M_\odot$ at the last measured point. Uson & Matthews (2003) reach a very similar conclusion. UGC7321 has a similar dark-to-light mass ratio, although it is significantly more massive than DDO154 and shows evidence of a bar (Carignan & Freeman, 1988).

The dominance of the halo at all radii means that the stellar mass-to-light ratio is rather unconstrained. Forcing a maximum disk fit yielded a stellar M/L_R of 2.9, but resulted in a very poor fit with rotation velocities in error by 15-25% in the inner disk. Even with a maximum disk fit, the peak rotation for the stellar disk was only 43 km s^{-1}. The best fit occurs for an M/L_R of 1.05, but all M/L_R values less than 1.05 provide acceptable fits to the rotation curve. Consequently, we use 1.05 as an upper limit in the analysis in Sect. 3.

The low mass-to-light ratio and extremely sub-maximal nature of the UGC7321 stellar disk implies that the recent star formation rate exceeds the average rate over the galaxy's lifetime. Observations by Matthews et al. (1999) that found a significant fraction of young stars support our results. Detailed studies of the vertical disk structure indicate multiple disk components (Matthews, 2000). Our finding of a very low mass-to-light ratio (in the *R*-band) warrants further studies of the structure and composition of the stellar disk, but this is beyond the scope of the present paper.

3. Method for fitting the halo shape

The thickness of the gas layer depends on the vertical force K_z, and hence on the shape of the dark matter halo (Maloney, 1992; Olling & van Gorkom, 1993; Kundic et al., 1993; Maloney, 1993). A gas layer with less flaring for a given gas velocity dispersion implies a stronger K_z.

Analytically it has been shown that at large radii the thickness of the gas layer is roughly proportional to the square root of the halo flattening q (Maloney, 1993; Olling, 1995) and that the flaring should increase radially in an exponential fashion (van der Kruit, 1981). This was confirmed in our measurements and the earlier study of Rupen (1991) comprising high resolution VLA HI observations of NGC891 and NGC4565.

We determine the halo flattening by measuring the z-gradient of the total vertical force $K_{z,tot}(R,z)$ from the equation of hydrostatic equilibrium for the gas layer, and evaluating dK_z/dz for each luminous mass component using Poisson's equation. The halo gradient $dK_{z,h}/dz$ is modelled using the equation for the vertical force K_z of a flattened pseudo-isothermal halo given in Sackett et al. (1994).

Given the gas disk is in equilibrium, the gas pressure gradient and internal forces must exactly balance the gradient of the total gravitational potential of the galaxy, where the total gravitational potential Φ_{tot} is the sum of the stellar, gas and halo potentials, $\Phi_{tot} = \Phi_h + \Phi_s + \Phi_g$. Assuming that the gas velocity dispersion

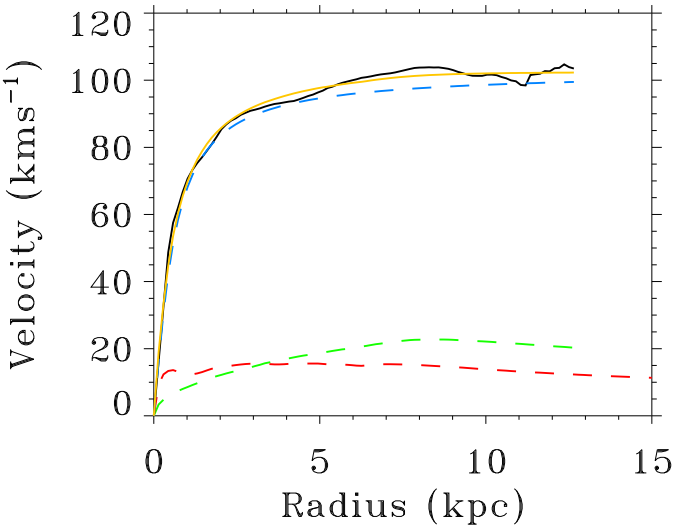

Fig. 5. Rotation curve decomposition of UGC7321. The observed rotation curve is shown by the thick (black) line, while the rotation due to the other components are shown by dashed lines; from the bottom up stars (red), gas (green) and the halo (blue). The disk has in this fit an M/L_R of 1.05. The resulting fit, $v^2_{fit} = v^2_g + v^2_s + v^2_h$, is shown by the grey full-drawn line (yellow).

.

is isothermal in z (though not in R), the equilibrium condition in z becomes

$$\frac{\partial^2}{\partial z^2}[\sigma^2_{v,g}(R)\ln\rho_g(R,z)] = \frac{\partial K_z(R,z)}{\partial z}. \quad (14)$$

If we further assume that the gas density distribution is Gaussian in z, the vertical gradient of the total K_z becomes a simple function of the gas velocity dispersion and the vertical FWHM thickness of the gas, both functions of radius which we measured in paper III, namely

$$\frac{\partial K_{z,tot}(R,z)}{\partial z} = -\frac{\sigma^2_{v,g}(R)}{(\mathrm{FWHM}_{z,g}(R)/2.355)^2}. \quad (15)$$

From this we see that the vertical gradient of $K_{z,tot}$ derived from such a gas disk is constant in z, and varying in R.

The gradient of the vertical force of each of the luminous components was directly calculated from the Poisson equation for each component

$$\frac{\partial K_z(R,z)}{\partial z} = -4\pi G\rho(R,z) + \frac{1}{R}\frac{\partial(RK_R)}{\partial R}, \quad (16)$$

where $\rho(R,z)$, K_R, and K_z correspond to the volume density and forces of that component. In terms of $v^2(R)$, the squared rotation due to that mass component, we can rewrite this as

$$\frac{\partial K_z(R,z)}{\partial z} = -4\pi G\rho(R,z) + \frac{1}{R}\frac{\partial v^2(R)}{\partial R}. \quad (17)$$

Consequently, the gradient of the halo force must satisfy

$$\frac{\partial K_{z,h}(R,z)}{\partial z} = \frac{\partial K_{z,tot}(R,z)}{\partial z} - \frac{\partial K_{z,s}(R,z)}{\partial z} - \frac{\partial K_{z,g}(R,z)}{\partial z}, \quad (18)$$

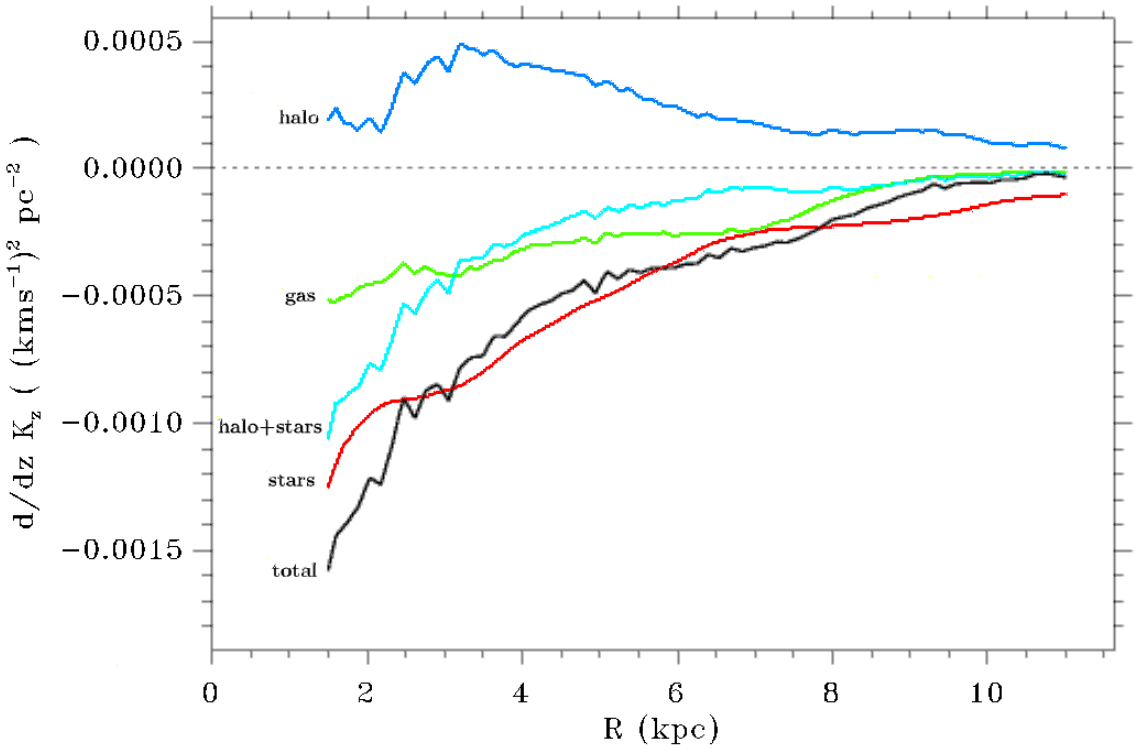

Fig. 6. The vertical gradient of the vertical force. The total gradient, $dK_{z,tot}/dz$ determined from hydrostatics is shown as the thick, black line (labelled 'total'), while the gradients for the gas and stars is shown in green and red (and labelled 'gas' and 'stars'), respectively. The stellar gradient $dK_{z,s}/dz$ is calculated using the stellar mass-to-light ratio of $M/L_R = 1.05 \pm 0.33$, derived from rotation curve decomposition. This value of the stellar M/L_R is clearly too high as the gradient allowed for the halo (shown in blue and labelled 'halo') is positive at all radii, requiring negative halo densities. The stellar M/L_R needs to be reduced to allow a negative halo gradient $dK_{z,h}/dz$. The cyan line (labelled 'halo+stars') shows the sum of stellar and halo components determined by $dK_{z,tot}/dz - dK_{z,g}/dz$, which must be fitted with a non-negligible stellar M/L_R and a positive density halo.

where the subscripts s, g and h, denote the stars, gas and halo, respectively.

The vertical $\partial K_{z,h}(R,z)/\partial z$ force of the flattened pseudo-isothermal halo is given in Sackett et al. (1994). As the asymptotic halo rotation and the halo core radius were well determined from the rotation curve decomposition, and the central density determined by q, the fitting of $dK_{z,h}/dz$ reduces to a fit with a single parameter q.

Comparison of the stellar vertical force gradient with the total vertical force gradient shows that the vertical force puts a much stronger constraint on the stellar mass-to-light ratio than does the radial force fitting undertaken in rotation curve decomposition. Inclusion of the gas self-gravity requires that the stellar vertical force gradient $dK_{z,s}(R,z)/dz$ must be

$$\frac{dK_{z,s}(z)}{dz} < \frac{dK_{z,tot}(z)}{dz} - \frac{dK_{z,g}(z)}{dz} \tag{19}$$

where from here on we take the R-dependence of K_z as implicit and write the derivatives as total derivatives.

Given that the stellar mass density and its squared rotation are both proportional to the stellar mass-to-light ratio, we see from Eqn. (17) that the vertical gradient of the vertical force of the stars is linearly related to the stellar mass-to-light ratio. As the low stellar luminosity meant the rotation curve decomposition was relatively insensitive to the stellar mass-to-light ratio, we consider the stellar mass-to-light ratio to be a free parameter and fitted

$$\frac{dK_{z,tot}}{dz} - \frac{dK_{z,g}}{dz}$$

as determined from the observations as a function of R with

$$\frac{dK_{z,h}}{dz} + \frac{dK_{z,s}}{dz},$$

where the $K_{z,h}$ is modelled by the flattened pseudo-isothermal halo and the z-gradient of the stellar vertical force is

$$\frac{dK_{z,s}}{dz} = \left(\frac{M}{L}\right)\frac{dK_{z,s}}{dz}\bigg|_{M/L_R=1}.$$

The total K_z gradient and the gas K_z gradient come directly from observations without any free parameters.

We recall from above that the vertical gradient of $K_{z,tot}$ derived for a Gaussian gas disk is independent of z. To be most sensitive to the constraints from the luminous mass density, we fit the gradient of the vertical force near the midplane at $z = 100$ pc, high enough to avoid the bulk of the internal extinction caused by dust in the plane of the thin stellar disk.

4. The halo shape of UGC7321

4.1. Results of the fitting

Fig. 6 shows the vertical gradient of each of the K_z components for UGC7321. The thick, black line (labelled 'total') is the gradient determined from the gas flaring and velocity distribution using Eqn. (15). The gradient due to the stellar disk is shown by the red line (labelled 'stars') and has been calculated with the mass-to-light ratio of 1.05, which was the best fitting value in our rotation curve decomposition. We see immediately that the

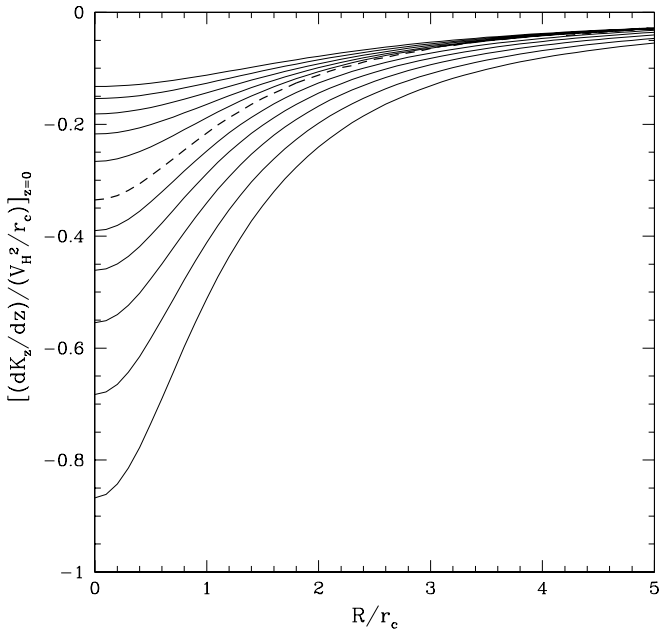

Fig. 7. The vertical gradient equated near the midplane of a flattened pseudo-isothermal halo, as calculated from Eqn. (6) of Sackett et al. (1994) for both oblate and prolate halos ranging from q of 0.5 to 1.5 in steps of 0.1. The bottom curve corresponds to the most flattened halo with $q = 0.5$, becoming increasingly shallow as the halo gets less flat. The gradient of a spherical halo is shown by the dashed line. The top curve corresponds to $q = 1.5$.

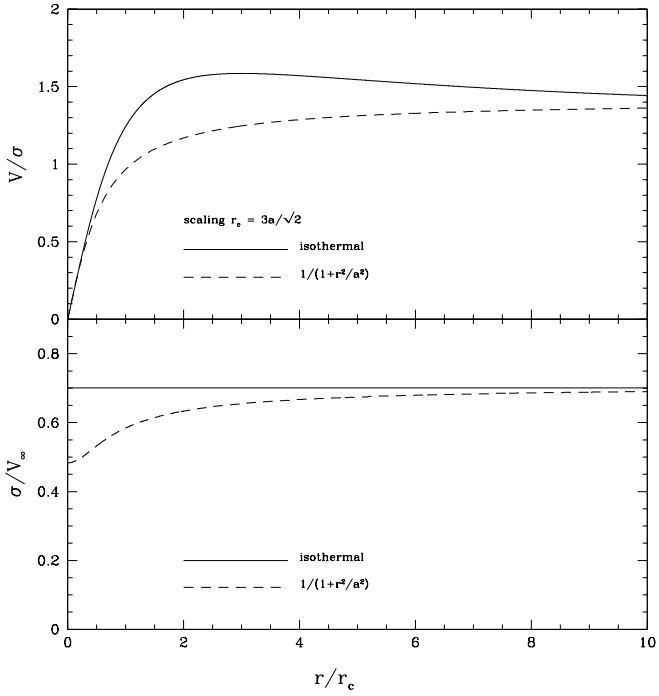

Fig. 8. This figure shows the difference in the rotation curve and velocity dispersion of isothermal and pseudo-isothermal halo models. The top panel shows that rotation of an IT halo rises above the asymptotic rotation speed at large radii, before declining to it, while the rotation curve of a PIT halo approaches the asymptotic rotation from below. Both rotation curves are scaled to the same asymptotic rotation speed to allow comparison. The lower panel shows that an isotropic pseudo-isothermal halo is not isothermal, exhibiting a lower velocity dispersion at low radii. (Adapted from Fig. 1 of Kormendy & Freeman, 2004.)

stellar $dK_{z,s}/dz$ alone is comparable to the total $dK_{z,tot}/dz$ given by the hydrostatics over most of the range of R. The gradient due to the HI is the line labelled 'gas' (green). We can subtract this gradient for the gas from the total gradient and derive the gradient due to the sum of the halo and the stars. This is the (cyan) line labelled 'halo+stars'. Subtracting the gradient for the stars from the gradient for the (halo + stars) then leaves the gradient that should be attributed to the halo alone (blue line labelled 'halo'). With the adopted M/L ratio for the stellar disk, the halo gradient turns out to be positive, which is unphysical.

From this example, it is clear that the gradient of $K_{z,tot}$ measured from the hydrostatics provides a very strong constraint on the stellar M/L_R ratio. Even with a zero-mass halo, which is excluded by the rotation curve fit, we see that the stellar M/L_R must be less than 1 to leave room for the gradient of K_z given by the gas self-gravity. With the necessary inclusion of the gas, we find that the stellar mass-to-light ratio M/L_R must be $\lesssim 0.6$. The difference $dK_{z,tot}/dz - dK_g/dz$ (cyan; labelled 'halo+stars') constitutes the combined dK_z/dz of the halo (blue; labelled 'halo') and stars (red; labelled 'stars'). The rotation curve decomposition requires a positive halo mass density at all radii, thus $dK_{z,h}/dz < 0$ for all radii. This constraint requires that the stellar $M/L_R \ll 1$.

Inspection of the $dK_{z,tot}/dz - dK_{z,g}/dz$ difference (cyan; 'halo+stars') shows a steep gradient at small R, flattening at large radii, particularly where the gas layer undergoes exponential flaring at radii outside 7 kpc. We see from Fig. 7 that this is similar to the characteristic shape of $dK_{z,h}/dz$ for pseudo-isothermal halos with different halo flattenings. But despite this similarity, it was not possible to fit the halo flattening q while holding the core radius R_c and the asymptotic halo rotation $v_{h,\infty}$ fixed, even with a zero mass stellar distribution (stellar $M/L_R = 0$) and allowing q to range between oblate and prolate shapes. By adjusting q, and keeping $M/L_R|_{stars}$ small, it is possible to get a similar shape to the difference gradient (cyan; 'halo+stars'), but it is always offset to larger negative values of the gradient. This implies that the asymptotic halo rotation scale derived from the rotation curve is too high, as the magnitude of $dK_{z,h}/dz$ is proportional to the $v^2_{h,\infty}$ (see Sackett et al., 1994).

This may be an artefact of the adopted pseudo-isothermal halo model. While the flattened pseudo-isothermal (PIT) model is computationally convenient, we note that a true (spherical) non-singular isothermal (IT) model was initially adopted for dark halos (Carignan & Freeman 1985, 1988). Few studies have compared the relative merits of the PIT and IT dark halo models. In their paper on halo scaling laws for disk galaxies (Sc and later) and dwarf speroidals, Kormendy & Freeman (2004) compare halo fits to rotation curves over a large sample and generate scaling laws between halo parameters measured with a IT halo and those with a PIT halo. In Fig. 8 (adapted from Fig. 1 of Kormendy & Freeman, 2004), we show IT and PIT halo rotation scaled to the same asymptotic rotation. As can be seen, the rotation of the IT halo rises above the asymptotic rotation speed before declining to it at large radii, while the rotation curve of a PIT halo approaches the asymptotic rotation from below. The declining shape of the rotation curve for the IT model would provide a lower and possibly more realistic estimate of the asymptotic rotational velocity $v_{h,\infty}$ from a rotation curve decomposition of rotation data which in practice does not extend to radii in excess of a few halo core radii.

If an IT halo was fitted to the observed rotation curve of UGC7321, the asymptotic rotation would be approximately 20-

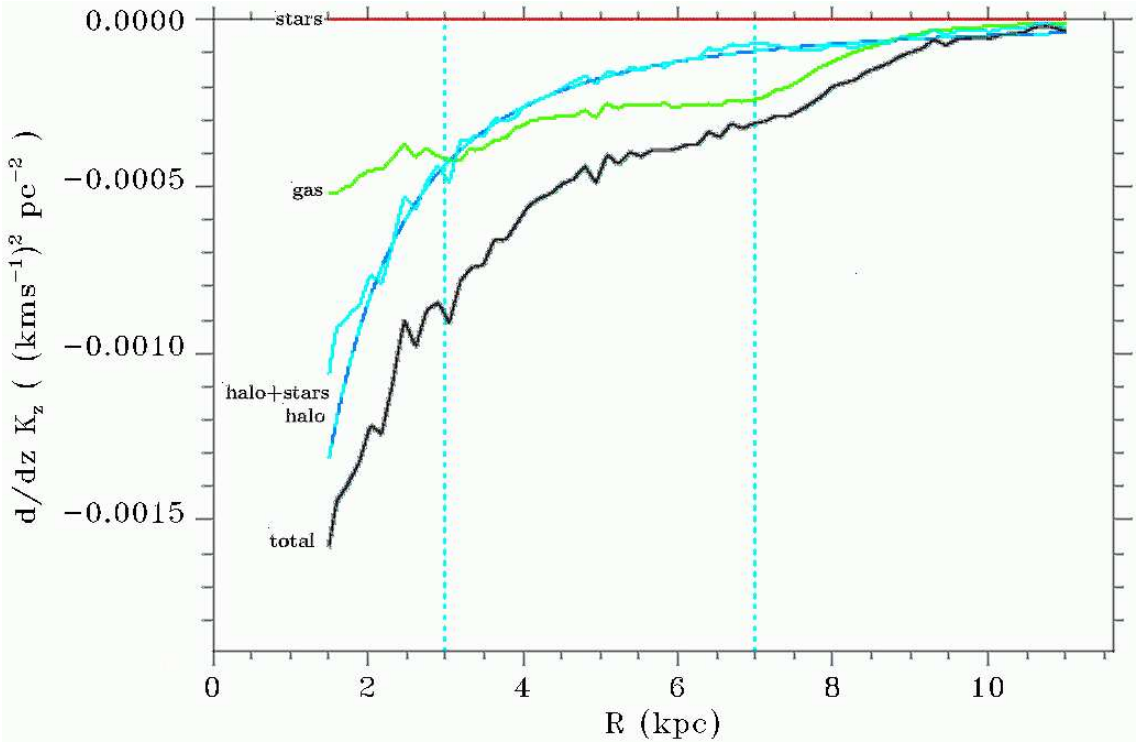

Fig. 9. The z-gradient of the vertical force showing successful fits of the halo shape for a zero mass disk $M/L_R = 0$. The black curve, labelled 'total' shows the total gradient $dK_{z,tot}/dz$ derived from hydrostatics. The green ('gas') and red (coincident with the abcissa at the top of the figure) curves show the z-gradient derived using Poisson's equation for the gas and stellar mass components. The cyan ('halo+stars') line shows the difference $dK_{z,tot}/dz - dK_{z,g}/dz$. This line is fitted by the halo gradient $dK_{z,h}/dz$ which is modelled by a flattened pseudo-isothermal halo. To achieve a successful fit to the cyan line, the asymptotic halo rotation was scaled down by 30%. The measured halo flattening was $q = 1.0 \pm 0.1$. The vertical dotted (cyan) lines show the radial regime used for the fit.

40% lower than that of the PIT halo. This would provide the lower asymptotic rotation scale $v_{h,\infty}$ necessary to fit the difference dK_z/dz of UGC7321 with a flattened halo over radial ranges from 1.5 to 9 kpc.

Flattened non-singular isothermal halos could be formed by halo rotation or anisotropy of the velocity dispersion. The rotation is unlikely to be figure rotation, as figure rotation of triaxial halos measured in n-body simulations was found to be very slow (Bailin & Steinmetz, 2004) ($0.148\,h$ km s^{-1} kpc^{-1}, where h is $H_0/100$, insufficient to flatten halos more than $q \sim 0.7$). The velocity dispersion anisotropy of the halo dark matter would allow either prolate or oblate halos, just as velocity anisotropy of the stars in the brighter elliptical galaxies defines the galaxy shape.

With the asymptotic rotation as a free parameter in addition to the stellar M/L_R and q, we found that the residual dK_z/dz curve ('halo+stars', cyan) is best modelled with a halo shape of $q = 1.0 \pm 0.1$. Robust least squares minimization fitting using a Levenberg-Marquardt algorithm (MINPACK-1) favoured a zero mass stellar disk, but fits were almost as good for an $M/L_R = 0.2$ stellar disk. These fits were successful over the radial range from 2 – 9 kpc.

We illustrate this first for the unphysical case where there is no mass in stars in Fig. 9. This figure is organised in the same manner as Fig. 6. The gradient due to the stars is now zero at all z. Recall that the (cyan) line 'halo+stars' is the observed gradient, which has to be fit. The smooth (also cyan) line 'halo' is that fit (the dashed -blue- line superimposed is that of the halo alone, which is the same when M/L_R is zero). This best fit was achieved with an asymptotic PIT halo rotation reduced by 30 ± 5% compared to the PIT fit to the rotation curve in Fig. 5.

It is remarkable that the shape of the R-dependence of dK_z/dz for the adopted halo model in Fig. 9 agrees so well with the shape of the K_z gradient derived from the HI flaring and velocity dispersion, at least for radii < 9 kpc. Although some rescaling of the *strength* of the K_z force was needed, we see that the density distribution of the adopted spherical PIT, using the core radius derived from the rotation curve fit, also provides the correct radial variation of the K_z gradient. This need not have happened. Although the K_R estimate from the rotation curve and the hydrostatic estimate of dK_z/dz come from analysing the same XV data (see paper III), the two functions come from different features in the XV data, so are relatively independent.

In Fig. 10 we show the fit for a stellar $M/L_R = 0.2$ disk. The lines labelled 'halo+stars' (cyan) show the gradient as deduced from the observed total gradient minus that of the gas in the full-drawn line (which of course is the same as in Fig. 9) and that of the sum of the gradient of the halo model fit and that deduced from the stellar distribution with $M/L_R = 0.2$ as the dashed line. The gradient from the stellar disk alone is the (red) curve labelled 'stars' and for the halo the (blue) curve labelled 'halo'. For this case an asymptotic halo rotation reduction of 50 ± 5% was needed. In effect, reducing $v_{h,\infty}$ and reducing the stellar M/L_R have similar effects of increasing the magnitude of the asymptotic value of the difference dK_z/dz curve ('halo+stars',cyan). For both cases ($M/L_R = 0$ in Fig. 9 and $M/L_R = 0.2$ in Fig. 10), the shape of this difference dK_z/dz curve dictated (given the derived core radius for the dark halo from our rotaton curve decomposition) a halo flattening close to spherical.

At radii larger than 9 kpc, the strong flaring causes the difference dK_z/dz (cyan, 'halo+stars') to be too small to be fit with

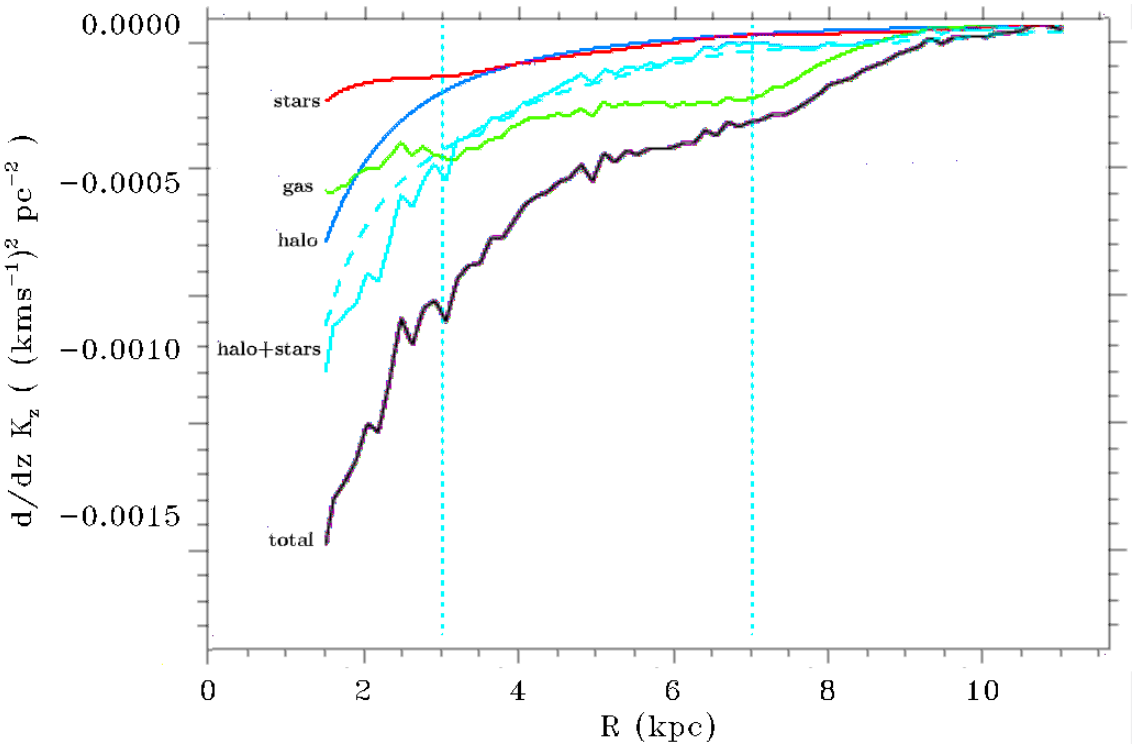

Fig. 10. The z-gradient of the vertical force showing successful fits of the halo shape for stellar mass-to-light ratio M/L_R = 0.2. The curve are coloured as in Fig. 9, except that the line for the stars is now at non-zero values. The cyan line, labelled 'halo+stars', shows again the difference $dK_{z,tot}/dz - dK_{z,g}/dz$ which is fitted by the stellar gradient $dK_{z,s}/dz$ derived from Poisson's equation and the halo gradient $dK_{z,h}/dz$ which is modelled by a flattened pseudo-isothermal halo. To achieve a successful fit to this line, the asymptotic halo rotation was scaled down by 50%. The thin full-drawn (blue) line, labelled 'halo' corresponds to this halo, while the dashed (cyan) line shows the gradient due to this halo and that of the stars together. A stellar mass-to-light ratio significantly larger than 0.2 was not possible. Again, the measured halo flattening was $q = 1.0 \pm 0.1$. The vertical dotted (cyan) lines show the radial regime used for each fit.

the same asymptotic halo rotation. Even the shallow gradient of dK_z/dz given by a highly prolate halo, combined with a low $v_{h,\infty}$, did not produce a good fit at these radii. We briefly discuss why the derived gradient for halo+stars may have been underestimated.

We have argued that a true isothermal halo may provide a more valid model for this analysis. Another possibility is that the gas velocity dispersion is not vertically isothermal. We were forced to adopted this assumption in the hydrostatic equation, because there is currently no available measurements of the z-dependence of the gas velocity dispersion.[1] Prior to our work the gas velocity dispersion had only been measured in a few face-on galaxies. Our HI disk modelling of edge-on galaxies has more than doubled the number of galaxies with radial gas velocity dispersion measurements. These high resolution observations show that the gas velocity dispersion is not isothermal in radius, but its vertical properties are unknown and we had to assume that is is vertically isothermal.

The gas velocity dispersion in disk galaxies is often ascribed to local heating by supernovae and stellar winds in star formation regions. Indeed, Shostak & van der Kruit (1984) found in NGC628 that the gas velocity dispersion is systematically higher in the spiral arms than in between. On the other hand, similar velocity dispersions are seen in regions of star formation and in regions where there is no visible star formation (e.g. Meurer et al., 1996), and both low and high surface brightness galaxies seem to have similar gas velocity dispersion. Sellwood & Balbus (1999) offer a plausible alternative, suggesting that weak magnetic fields in galaxies allow energy to be extracted from differential rotation via MHD-driven turbulence. This would result in a gas velocity dispersion that was proportional to the rotational shear due to the disk, resulting in similar gas velocity dispersion for galaxies with similar rotation curves. However, while heating caused by gas shear could generate radial variation in the gas velocity dispersion, it is unclear how it could cause the gas velocity dispersion not to be vertically isothermal. Conversely, the decline in star formation away from the midplane could cause a fall-off in gas velocity dispersion with z.

A non-isothermal vertical gas velocity dispersion would probably have more of an effect at larger radii where the flaring gas is probing a larger range in z. A gas velocity dispersion declining with z would increase the absolute total vertical gradient of K_z derived from the equation of hydrostatic equilibrium. A significant increase of $dK_{z,tot}/dz$ would enable a larger asymptotic halo rotation more consistent with a pseudo-isothermal halo and a larger stellar M/L_R.

Another, less plausible, explanation of the dK_z/dz fitting problem at large radius, is that the gas-to-HI ratio used to scale the HI density to account for He and H_2 is not constant. This is unlikely as the He content is mainly primordial and well known from big bang nucleo-synthesis. As He accounts for 0.34 of the additional 0.4 fraction, it is unlikely that a radially declining molecular hydrogen distribution could significantly reduce $dK_{z,g}/dz$ thus allowing a higher difference dK_z/dz (cyan).

[1] Because of S/N limitations, our measurement of the gas velocity dispersion in paper III models the HI XV diagram integrated over z. Thus it represents a luminosity-weighted average dispersion as a function of radius.

5. Comparison to other work

We first review earlier work on the flattening of dark halos in spiral galaxies. The earliest concern was whether the dark matter indicated by flat rotation curves resided indeed in a more or less round halo or was part of the disk. That the latter was not the case was shown in 1981, using evidence from bulge isophotes in external galaxies and star counts in our Galaxy (Monet et al., 1981) and from HI flaring in NGC 891 (van der Kruit, 1981). Next, the question of the actual flattening $q = c/a$ of dark halos in spiral galaxies arose and we will now review previous work on this subject, starting with our Galaxy. One of the early methods is the analysis of the local surface density in the Solar neighbourhood using stellar kinematics. With this method Binnet et al. (1987) find $0.3 \leq q \leq 0.6$, van der Marel (1991) $q \geq 0.34$ and Bienaymé et al. (2006) $q \gtrsim 0.5$.

At large radial distances of $8.0 \leq R \leq 60$ kpc, RR Lyrae stars show the dark matter distribution to be flattened by $q \sim 0.7$ (Amendt & Cuddeford, 1994). Hyper-velocity stars open another promising way of probing the shape of the Galactic dark matter distribution. One star, assuming it is 70 kpc away, gives $0.5 < q < 1.6$ (Gnedin et al., 2005). Samurović et al. (1999) used the microlensing optical depth towards the Galactic bulge, LMC, SMC and M31 to probe the shape of the Galactic halo to large radii ($R \leq 5R_{25}$). However, they were not able to derive strong constraints: $q = 0.6 \pm 0.4$.

Since the discovery of the Sagittarius dwarf galaxy, modelling of its extended stellar tidal debris stream has become one of the most promising methods. Majewski et al. (2003) show that the Sagittarius stream traces a great circle around our Galaxy, extending to radii of $2R_{25}$ from the Galactic centre. If the tidal debris has made several orbits, the Galactic halo must be near-spherical so that the stream does not precess away from a single plane. Merrifield (2004) argued that the apparent coherency of the carbon star kinematics in the stream suggest that all the stars are on the same wrap, making it impossible to constrain the halo flattening. Conversely, Ibata et al. (2001) contend that the stream has made several orbits, and from this infer that the Galactic halo must have flattening $q \gtrsim 0.7$ in the radial range $16 < R < 60$ kpc.

Recently, numerically modelling of small satellite infall on a Sgr-like orbit by Helmi (2004a) finds that tidal streams younger than about 2 Gyr lead to spatially coherent streams for a large range of halo flattenings $0.6 \leq q \leq 1.6$. Since then she (Helmi, 2004b) has significantly revised her initial measurement to a highly prolate shape with $1.25 \lesssim q \lesssim 1.5$ by constraining the star sample to the older Sgr stream stars of Law et al. (2005). However, Johnston et al. (2005) dispute this result, finding a near-spherical halo with $q \sim 0.83 - 0.92$. In a more recent analysis of the Magellanic Stream Růžička et al. (2007) find a flattening of $0.74 \leq q \leq 1.20$.

The situation for halo shape measurement in external galaxies is just as confusing, because some methods are suited only to specific types of galaxies. The determination of halo shape from polar ring galaxies is such a case. By simply comparing the equatorial and polar rotation curves it is possible to ascertain the flattening of the total potential. Using this method NGC4650A and A0136-0801 were found to be moderately flattened with $q \gtrsim 0.7$ (Whitmore et al., 1987; Schweizer et al., 1983, respectively), while MCG-5-7-1 was found to be approximately spherical (Whitmore et al., 1987). A potentially more accurate method is to model the rotation along both axes using a multi component mass model comprising bulge, equatorial stellar and gas disks, and polar stellar and gas rings. Using this method, Sackett & Sparke (1990) originally found the halo flattening of NGC4650A to be $0.3 \leq q \leq 0.7$; subsequent higher quality observations were able to constrain the halo more tightly, to $0.3 \leq q \leq 0.4$ (Sackett et al., 1994). This method has also been applied to AM2020-504, where the flattening was found to be $q \sim 0.6$ (Arnaboldi et al., 1993). Another method involves modelling of the twisting caused by precession of the ring. With some specific assumptions, Steiman-Cameron et al. (1992) constrain the flattening of the NGC4753 halo to be $0.84 \leq q \leq 0.99$. Finally, using the twisting of the morphological minor axis of the disk plane away from the kinematic minor axis to model the velocity field of polar rings, the flattening of the dark halo of A0136-0801 was found to be $q \sim 0.6$ (Sackett & Pogge, 1995).

Another method that has been used to measure halo flattening is strong gravitational lensing. An early study of a double lens system comprising two spirals found $q \gtrsim 0.4$ (Koopmans et al., 1998). More recently there have been two studies of multiple quad lens systems finding $q \gtrsim 0.4$ (Rusin & Tegman, 2110) and $q \sim 0.7$ (Cohn & Kochanek, 2004), and another analysis of a double lens system $0.6 < q < 0.7$ (Chae et al., 2002).

Warps in stellar disks (e.g. Reshetnikov & Combes, 1998) offer several mechanisms to probe the halo shape of spiral galaxies. One method uses the precession of the warped disk to constrain the halo flattening. It has been applied to NGC2903, yielding a halo flattening of $q = 0.80 \pm 0.15$ (Hofner & Sparke, 1994).

It is also possible to measure the mean shape of vast numbers of galaxies via weak gravitational lensing. Measurements of about 10^5 lensed systems against about 10^6 background galaxies (Hoekstra et al., 2005) find a mean projected halo ellipticity of $0.20^{+0.04}_{-0.05}$ and a mean projected halo flattening of $\langle q \rangle = 0.66^{+0.04}_{-0.06}$ (1-σ error) . However, a larger investigation of about 2 million lensed galaxies against 32 million background galaxies from the SDSS dataset found no strong evidence of flattening, with $\langle q \rangle = 0.99^{+0.06}_{-0.05}$ (Mandelbaum et al., 2006).

The results of halo flattening studies so far do not reveal a consistent picture. We believe that the method of the flaring of the gas layer is among the most promising, at least for late-type spiral galaxies. First tried by Celnik et al. (1979) on the Galaxy, early development of the method was undertaken by van der Kruit (1981) who applied it to low resolution observations of NGC891, concluding that the halo was not as flattened as the stellar disk. It was then applied to several galaxies in the 1990's, most notably the careful study of the very nearby Sc galaxy NGC4244, which found a highly flattened halo with by $q = 0.2^{+0.3}_{-0.1}$ out to radii of $\approx 2R_{25}$ (Olling, 1996). All applications of the flaring method have indicated highly flattened halo distributions with $q \leq 0.5$ (Becquaert, 1997; Becquaert & Combes, 1997; Sicking, 1997). Recently, Banerjee & Jog (2008) measured a flattening of $q = 0.4$ from flaring of the HI layer in M31. This assumed a constant HI velocity dispersion with radius; if it is allowed to have a modest decline in the outer disk the flattening can be made less with q more like 0.5 to 0.6. With the exclusion of NGC4244, it may therefore be suspected that the assumption of a radially constant gas velocity dispersion has led to errors in the derived flattening of the halo.

Measurements of significant flattening using the flaring method initially led to the supposition that perhaps the method is systematically biased to flattened halos. Our analysis of UGC7321 shows that this is not the case: the gas layer flaring method is just as sensitive to prolate halos as it is to oblate ones. Here, we briefly consider the set of q measurements using the flaring method that have indicated flat halos. The flattening for NGC891 (Becquaert & Combes, 1997) was estimated from VLA observations with a low peak signal-to-noise of 13 (Rupen, 1991). The low sensitivity could have led to underestimates of

the gas density and vertical flaring, thus changing the shape of both $dK_{z,tot}/dz$ and $dK_{z,g}/dz$, and thereby q. Except in the case of NGC4244 (Olling, 1996), it is unclear what model was used for the radial gas velocity dispersion. An assumption of radially-constant gas velocity dispersion could easily skew the derived halo shape measurement.

In some cases it is not clear whether the gas self-gravity was included in the mass modelling. Additionally, excluding NGC4244, all the previous measurements of the halo flattening from the gas layer flaring were performed on large Sb-Sc galaxies with maximum rotation speeds v_{max} between 177 and 295 km s^{-1}. As the gas layer flaring is inversely proportional to v_{max}, the maximum HI flaring of these galaxies is $\lesssim 1$ kpc, making it difficult to resolve unless the galaxy is nearer than 5 Mpc.

The Galactic q measurement from the gas flaring by Olling & Merrifield (2000) is particularly interesting. They were unable to fit the halo with a pseudo-isothermal model, unless the Solar radius and rotation velocity are significantly less ($R_\odot \leq 7.6$ kpc, $\Theta_\odot \leq 190$ km s^{-1}) than the standard values. The uncertainty associated with these values translates to a large uncertainty of q: $q = 0.8 \pm 0.3$.

UGC7321 is the least massive galaxy for which the halo flattening has been measured. The derived R-band face-on central surface brightness is 2.5 times fainter than the B-band measurement of NGC4244, and the total R-band luminosity is 4.5 times fainter than NGC4244, while its gas layer flares to twice the height of NGC4244. The very low stellar mass of UGC7321 made it an ideal candidate for halo modelling with the gas flaring method.

Although there are now a number of different measurements of galactic halo flattening, there is no obvious concentration around a particular halo shape or any correlation of halo flattening with galaxy morphology. Currently the measured q values range from 0.1 to 1.4. The low q values for the large Sb galaxies, M31, NGC891 and NGC4013, are puzzling as in these cases the stellar density distribution may be more spherical than the halo density distribution. It seems unlikely that the galactic halos could exist in the range of shapes measured, unless the fractions of the constituent dark matter types vary significantly from galaxy to galaxy. Early work by Dubinski (1994) found that including baryon infall in n-body halo simulations led to nearly axisymmetric halos. Most n-body simulations without hydrodynamics tend to form prolate halos (Sellwood, 2004); however, new work by Dubinski (unpublished) has shown that the inclusion of hydrodynamical modelling generates halos that are more spherical.

We note here an application of HI hydrostatics to our Galaxy by Kalberla et al. (2007), which illustrates the potential power of HI hydrostatics to trace the Galactic potential gradient and hence the total dark matter distribution in the Galaxy. Kalberla et al. adopted an isothermal velocity dispersion for the Galactic HI and found several components of dark matter, including the usual extended halo with a mass of about 1.8×10^{12} M$_\odot$, a thick self-gravitating disk with a mass of about 2 to 3×10^{11} M$_\odot$, and an outer dark matter ring with a mass of about 2 to 3×10^{10} M$_\odot$. Similar studies in other edge-on galaxies may reveal comparable substructure in the dark matter, including dark matter rings which may be left over from accreted and circularized smaller galaxies, drawn down into the disk by dynamical friction. As we will argue in the next section, it is important to measure the structure, rotation and velocity dispersion of the HI in both R and z, to ensure such structures are not artifacts of assumptions required to apply the hydrostatics.

Finally we note that since we submitted the original version of this paper, a study of the density distribution of dark matter halo of UGC 7321 by Banerjee et al. (2010) appeared, using the rotation curve and flaring of the HI layer derived from the same data. In this study the fitting was performed with the halo central density, core radius and radial exponential density slope as free parameters, but with the halo assumed spherical, the stellar M/L of the disk fixed and using values for the HI velocity dispersion from Gaussian fits to the position-velocity profiles (typically 7 to 9 km s^{-1}). These authors also conclude from their work that the dark matter halo dominates the dynamics of UGC 7321 at all radii, but they do not put constraints on the dark matter halo flattening.

6. Conclusions

In this study we have shown that it is possible to measure the gas flaring and HI velocity dispersion via modelling of the HI distribution. Using these methods we found that the small late-type disk galaxies in our sample show substantial HI flaring, increasing linearly with radius in the inner disk and exponentially in the outer disk. The HI velocity dispersion has a mean value of 7 km s^{-1}, but varies from 4.5 to 12 km s^{-1}. Our HI modelling method is also capable of measuring the vertical variation of the HI velocity dispersion given additional HI observations.

UGC7321, a small low surface brightness Sd galaxy in our sample, has the most accurate flaring measurements in our sample. We were unable to model the observations using a pseudo-isothermal halo. By lowering the asymptotic halo rotation to a value corresponding to a true isothermal halo model, we found that UGC7321 has a spherical halo density distribution of $q = 1.0 \pm 0.1$. Highly prolate halos ($q > 1.2$) and highly flattened halos ($q < 0.6$) are strongly excluded if our approximation of a true isothermal halo is valid.

Our mass modelling analysis assumed that the HI gas velocity dispersion was vertically isothermal, as no measurements of the vertical variation of the HI gas velocity dispersion are as yet available.[2] If the HI velocity dispersion is in fact vertically declining, this would lead to a larger estimated vertical gradient of the total vertical force, which may allow a pseudo-isothermal model for the halo.

UGC7321 is a gas-rich galaxy ($M_{HI}/L_R = 2.2$), with a very low stellar mass galaxy ($M = 3 \times 10^8$ M$_\odot$), four times less massive than the gas disk. The R-band stellar mass-to-light ratio of UGC7321 is very low at $M/L_R \lesssim 0.2$. Mass modelling of the vertical force distribution showed that vertical force fitting provides a much stronger constraint on the stellar mass-to-light ratio than the standard method of radial force fitting via rotation curve decomposition.

Two important assumptions in this work need to be tested further. The first is that the HI velocity dispersion is isothermal in z. For a definitive estimate of the R and z-components of the total potential gradients from HI hydrostatics, it is essential to have reliable measurements of the HI density, rotation and velocity dispersion as a function of both R and z. It should be possible, with additional short spacing ATCA observations supplementing our data, to measure the HI velocity dispersion as a function of z in ESO274-G001 by modelling the HI XV diagram at varying heights above the galactic plane. ESO274-G001 is the closest, isolated, southern edge-on galaxy at a distance of 3.4 Mpc. In

[2] Our measurements of the HI gas velocity dispersion used the vertically averaged HI distribution, ie. they are the luminosity-weighted mean velocity dispersion as a function of radius.

the northern hemisphere, UGC7321 is a prime candidate due to its high HI mass, despite its larger distance of 10 Mpc. The large HI flaring means that the HI could be measured at a height of 400 pc for radii from 5-11 kpc, and at 700 pc for radii from 9-11 kpc. The dwarf Scd galaxy NGC5023 is also an excellent candidate, given its distance of about 8 Mpc (van der Kruit & Searle, 1982). For this galaxy, early flaring measurements by Bottema et al. (1986) found that the gas thickness was constant with radius. This is a surprising result, because the v_{max} value for this galaxy is only about 80 km s^{-1}, and large flaring might be expected. It would be interesting to measure the radial and vertical variation of the gas velocity dispersion, gas flaring, and halo shape using beter data, as this galaxy has a similar size, HI brightness and total mass as UGC7321.

The other important test is to determine whether a true isothermal halo provides a better model than the pseudo-isothermal halo for the dark matter in late-type disk galaxies, or whether there are better models than either of these. Our analysis of UGC7321 has shown that the vertical gradient of the vertical force provides a significantly stronger constraint on the halo density distribution than does rotation curve decomposition. So, this test can in principle be achieved by analysing UGC7321 and the other galaxies in our sample with both flattened pseudo-isothermal and true isothermal halo models. Such flattened isothermal halos could be flattened by rotation or by anisotropy of the velocity dispersion. This will determine which kind of model is better for both the radial halo force as measured from the rotation curve, and the vertical force of the halo determined from dK_z/dz fitting.

Acknowledgements. We are very grateful to Albert Bosma who contributed greatly to initiating this project. He pointed out that HI flaring studies are best done on edge-on galaxies with low maximum rotational velocities, and we used an unpublished Parkes HI survey of edge-on galaxies by Bosma and KCF when selecting our galaxies. JCO thanks E. Athanassoula, M. Bureau, R. Olling, A. Petric and J. van Gorkom for helpful discussions. JCO is grateful to B. Koribalski, R. Sault, L. Staveley-Smith and R. Wark for help and advice with data reduction and analysis, and to P. Sackett, A. Kalnajs and F. Briggs for advice and discussions on the modelling. M. Pohlen generously provided his deep *R*-band image of UCG7321, for which we are very grateful. Scott Tremaine has our gratitude for a few important comments on a draft version of this paper. We thank the referee, J.M. van der Hulst, for his careful and thorough reading of the manuscripts of this series of papers and his helpful and constructive remarks and suggestions.

References

Amendt, P. & Cuddeford, P., 1994, ApJ, 435, 93
Arnaboldi, M., Capaccioli, M., Cappellaro, E., Held, E.V. & Sparke, L., 1993, A&A, 267, 21
Bailin, J. & Steinmetz, M., 2004, ApJ, 616, 27
Banerjee, A., & Jog, C.J., 2008, 685, 254
Banerjee, A., Matthews, L.D. & Jog, C.J., 2010, New Astr. 15, 89
Becquaert, J.-F., 1997, Ph.D. Thesis, University of Paris
Becquaert, J.-F. & Combes, F., 1997, A&A, 325, 41
Bienamyé, O., Soubiran, C., Mishenina, T.V., Kovtyukh, V.V. & Siebert, A., 2006, A&A, 446, 993
Binney, J., May, A. & Ostriker, J.P., 1987, MNRAS, 226, 149
Bottema, R., Shostak, G.S. & van der Kruit, P.C., 1986, A&A, 167, 34
Carignan, C. & Freeman, K.C., 1985, ApJ, 294, 494
Carignan, C. & Freeman, K.C., 1988, ApJ, 332, L33
Chae, K.-H., Biggs, A.D., Blandford, R.D., et al., 2002, Phys.Rev.Lett., 89, 151301
Celnik, W., Rohlfs, K. & Braunsfurth, E., 1979, A&A, 76, 24
Cohn, J.D. & Kochanek, C.S., 2004, ApJ, 608, 25
Dubinski, J., 1994, ApJ, 431, 617
Gnedin, O.Y., Gould, A., Miralda-Escude, J. & Zentner, A.R., 2005, ApJ, 634, 344
Helmi, A., 2004a, MNRAS, 351, 643
Helmi, A., 2004b, ApJ, 610, L97
Hoekstra, H., Yee, H.K.C. & Gladders, M.D., 2005. ApJ, 606, 67
Hofner, P. & Sparke, L.S., 1994, ApJ, 428, 466
Ibata, R., Lewis, G.F., Irwin, M., Totten, E. & Quinn, T., 2001, ApJ, 551, 294
Johnston, K.V., Law, D.R. & Majewski, S.R., 2005, AJ, 619, 800
Kalberla, P. M. W., Dedes, L., Kerp, J., Haud, U. 2007, A&A, 469, 511
Koopmans, L.V.E., de Bruyn, A.G. & Jackson, N., 1998, MNRAS, 295, 534
Kormendy, J. & Freeman, K.C., 2004, IAU Symp, 220, p.377
Kundic, T., Hernquist, H. & Gunn, J.E., 1993, AIP Conf. Ser. 278, 292
Law, D.R., Johnston, K.V. & Majewski, S.R., 2005, ApJ, 619, 807
Mandelbaum, R., Hirata, C.M., Broderick, T., Seljak, U. & Brinkmann, J., 2006, MNRAS, 370, 1008
Majewski, S.R., Skrutskie, M.F., Weinberg, M.D. & Ostheimer, J.C., 2003, ApJ, 599, 1082
Maloney, P., 1992, NASA Conf. Publ. 3190, p.117
Maloney, P., 1993, ApJ, 414,41
Matthews, L.D., 2000, AJ, 120, 1764
Matthews, L.D., Galagher, J.S. & van Driel, W., 1999, AJ, 118, 2751
Merrifield, M.R., 2004, IAU Symp. 220, 431
Meurer, G.R., Carignan, C., Beaulieu, S.F. & Freeman, K.C., 1996, AJ, 111, 1551
Monet, D.G., Richstone, D.O. & Schechter, P.L., 1981, ApJ, 245, 454
O'Brien, J.C., Freeman, K.C., van der Kruit, P.C. & Bosma, A., 2010a, A&A, submitted (Paper I)
O'Brien, J.C., Freeman, K.C. & van der Kruit, P.C., 2010b, A&A, submitted (Paper II)
O'Brien, J.C., Freeman, K.C. & van der Kruit, P.C., 2010c, A&A, submitted (Paper III)
Olling, R.P., 1995, AJ, 110, 591
Olling, R.P., 1996, AJ, 112, 481
Olling, R.P. & Merrifield, M.R., 2000, MNRAS, 311, 361
Olling, R.P. & van Gorkom, J.H., 1993, Third Teton Summer School, p.374
Pohlen, M., Balcells, M., Lütticke, R. & Dettmar, R.-J., 2003, A&A, 409,485
Pohlen, M., Dettmar, R.-J., Lütticke, R. & Aronca, G., 2002, A&A, 392, 807
Reshetnikov, V. & Combes, F., 1998, A&A, 337, 9
Rupen, M.P., 1991, AJ, 102, 48
Rusin, D. & Tegman, M., 2001, ApJ, 553, 709
Růžička, A., Palouš, J. & Theis, C., 2007, A&A, 461, 155
Sackett, P.D. & Pogge, R.W., 1999, AIP Conf. 336, 141
Sackett, P.D. & Sparke, L.S., 1990, ApJ, 361, 408
Sackett, P.D., Rix, H., Jarvis, B.J. & Freeman, K.C., 1994, ApJ, 436, 629
Samurović, S., Ćirković, M.M. & Milošević-Zdjelar, V., 1999, MNRAS, 309, 63
Schweizer, F., Whitmore, B.C. & Rubin, V.C., 1983, AJ, 88, 909
Sellwood, J.A., 2004, IAU. Symp 220, p.27
Sellwood, J.A.& Balbus, S.A., 1999, ApJ, 511, 660
Shostak, G.S. & van der Kruit, P.C., 1984, A&A, 132, 20
Sicking, F.J., 1997, Ph.D. Thesis, University of Groningen
Steiman-Cameron, T.Y., Kormendy, J. & Durisen, R.H., 1992, AJ, 104, 1339
Uson, J.M. & Matthews, L.D., 2003, AJ, 125, 2455
van der Kruit, P.C., 1981, A&A, 99, 298
van der Kruit, P.C. & Searle, L., 1982, A&A, 110, 61
van der Marel, R.P., 1991, MNRAS, 248, 515
Whitmore, B.C., McElroy, D.B. & Schweizer, F., 1987, ApJ, 314, 439